Tracking the spatial footprints of extreme storm surges around the coastline of the UK and Ireland

Paula Camus [a,b,*], Ivan D. Haigh [a], Niall Quinn [c], Thomas Wahl [d], Thomas Benson [e], Ben Gouldby [e], Ahmed A. Nasr [d], Md Mamunur Rashid [d,f], Alejandra R. Enríquez [d,g], Stephen E. Darby [h], Robert J. Nicholls [i], Norberto C. Nadal-Caraballo [j]

[a] *School of Ocean and Earth Science, National Oceanography Centre Southampton, University of Southampton, Waterfront Campus, European Way, Southampton, SO14 3ZH, UK*
[b] *Geomatics and Ocean Engineering Group, Departamento de Ciencias y Técnicas del Agua y del Medio Ambiente, E.T.S.I.C.C.P, Universidad de Cantabria, Santander, Spain*
[c] *Fathom Ltd., The Engine Shed, Station Approach, Bristol, UK*
[d] *Civil, Environmental, and Construction Engineering & National Center for Integrated Coastal Research, University of Central Florida, 12800 Pegasus Drive, Suite 211, Orlando, FL, 32816-2450, USA*
[e] *HR Wallingford, Howbery Park Wallingford, Oxfordshire, OX10 8BA, UK*
[f] *Division of Coastal Sciences, School of Ocean Science and Engineering, The University of Southern Mississippi, Ocean Springs, MS, 39565, USA*
[g] *Institute for Environmental Studies (IVM), Vrije Universiteit Amsterdam, 1081 HV, Amsterdam, Netherlands*
[h] *School of Geography and Environmental Sciences, University of Southampton, Highfield, Southampton, SO17 1BJ, UK*
[i] *Tyndall Centre for Climate Change Research, University of East Anglia, Norwich, NR4 7TJ, UK*
[j] *U.S. Army Corps of Engineers, Engineer Research and Development Center, Coastal and Hydraulics Laboratory, 3909 Halls Ferry Drive, Vicksburg, MS, 39180, USA*

ARTICLE INFO

ABSTRACT

Storm surges are the most important driver of flooding in many coastal areas. Understanding the spatial extent of storm surge events has important financial and practical implications for flood risk management, reinsurance, infrastructure reliability and emergency response. In this paper, we apply a new tracking algorithm to a high-resolution surge hindcast (CODEC, 1980–2017) to characterize the spatial dependence and temporal evolution of extreme surge events along the coastline of the UK and Ireland. We quantify the severity of each spatial event based on its footprint extremity to select and rank the collection of events. Several surge footprint types are obtained based on the most impacted coastal stretch from each particular event, and these are linked to the driving storm tracks. Using the collection of the extreme surge events, we assess the spatial distribution and interannual variability of the duration, size, severity, and type. We find that the northeast coastline is most impacted by the longest and largest storm surge events, while the English Channel experiences the shortest and smallest storm surge events. The interannual variability indicates that the winter seasons of 1989-90 and 2013–14 were the most serious in terms of the number of events and their severity, based on the return period along the affected coastlines. The most extreme surge event and the highest number of events occurred in the winter season 1989–90, while the proportion of events with larger severities was higher during the winter season 2013–14. This new spatial analysis approach of surge extremes allows us to distinguish several categories of spatial footprints of events around the UK/Ireland coast and link these to distinct storm tracks. The spatial dependence structures detected can improve multivariate statistical methods which are crucial inputs to coastal flooding assessments.

1. Introduction

Coastal floods are a major hazard globally that have an important compound dimension caused by tides, storm surge and/or waves, as well as even extreme precipitation and high river discharge (in certain locations, such as estuaries) (Zscheischler et al., 2020). This will be the

case with compound flood events that can occur from the interplay between riverine and coastal flood drivers in estuaries and deltas (Eilander et al., 2020). However, without the influence of a river, coastal flooding at any one time can be considered dependent on the total water level, which is a combination of multiple simultaneously occurring processes (i.e., astronomical tides, storm surges, wave setup, and seasonally and climatically varying mean sea level) that display a climate variability an order of magnitude greater than the global mean SLR signal (Anderson et al., 2019).

Many analyses of extreme sea levels consider only astronomical tides and storm surges (Haigh et al., 2016; Dullaart et al., 2021), or introduce the wave setup using a parametric approach based on offshore wave height (Vousdoukas et al., 2018; Kirezci et al., 2020). Coupled hydrodynamic-wave modelling on small areas with wide continental shelves during specific storms has demonstrated that the extreme sea levels are locally increased in the range of 0.1–0.2 m with high waves (7–10 m, Bertin et al., 2015), or that the wave setup contributes by up to 40% and 23% (Lavaud et al., 2020), even 71–120% (Pedreros et al., 2018) of the total maximum storm surges. A recent database of coastal extreme sea levels in the Mediterranean, using a coupled hydrodynamic-wave model, confirms that maximum sea levels could increase by up to 120% in the presence of waves (Toomey et al., 2022). Another wave effect in surges involves their impact on wind stress, often accounted for through wave-enhanced drag (Mastenbroek et al., 1993; Bertin et al., 2015, Pineau-Guillou et al). Simulations in the North Sea indicate that for young and rough sea states, considering wave-enhanced drag is crucial (Pineau-Guillou et al). However, this implies a wave-model coupling, which introduces complexity.

Interactions between mean sea level, tide, surge, and waves can reach several tens of centimeters (positive or negative) depending on the type of the morphology and hydrometeorological conditions (Idier et al., 2019). It has been observed that non-linear interactions between tide and surge can account for around 30% of the decrease in the extreme sea levels compared with the linear superposition of tide and storm surge traditionally applied in coastal impact studies (Arns et al., 1918). For instance, it has been noted along the North Sea coastline in the UK that the residual peak occurs everywhere 3–5 h before the nearest high water (Horsburgh and Wilson, 2007). Tide dependence of extreme water levels has also been detected along the French coast of the English Channel with a spatiotemporal variability which indicates a local character of the tide-surge interaction (Idier et al., 2012).

In terms of consequences, among all coastal flooding drivers, storm surges are the deadliest hazard at coasts (Enríquez et al., 2020). Many recent storm surge events (e.g., Cyclone Nargis in 2008 in Myanmar; Superstorm Sandy in 2012 along the US east coast; Typhoon Haiyan in 2013 in the Philippines) have caused considerable flooding, loss of life and destruction. The spatial extent of storm surge events is important as there are financial and practical implications for flood risk management, reinsurance, infrastructure reliability and emergency response, as impacts and losses may be spatially correlated. For example, in the UK and Ireland, the spatial extent of storm surges and coastal flood events was particularly remarkable around the coast during the exceptional winter of 2013-14 (Haigh et al., 2016).

The simultaneous flooding along extended coastal stretches, during the same storm, is commonly referred to as the event footprint (e.g., Haigh et al., 2016; Quinn et al., 2019, in the case of river flooding). During a storm event, the extreme sea level footprint varies along a given stretch of coastline, with sea levels being elevated in certain regions, but decreasing away from the main area of the storm's influence. However, the return period of extreme sea levels is typically considered constant in space when assessing coastal flooding impacts or risk. However, this assumption is only valid over local scales. This limitation could have significant implications for assessing coastal flood risk and could result in ineffective flood risk management decisions, such as emergency services or investment in flood defences (Wing et al., 2020).

Despite the importance of multi-site or along-coast dependence, only

a few analyses of the spatial footprints of storm surges or extreme sea levels have been conducted. Two studies have been performed at a regional scale along the UK coastlines (i.e., Haigh et al., 2016) and in New Zealand (i.e., Stephens et al., 2020), and there has been one global study to date (Enríquez et al., 2020). The two regional studies applied the same event-analysis based approach to sea levels (astronomical tide included) and skew surges using tide gauge measurements. In this approach, the 1 in 5-year return level of sea level or skew surge was identified by applying a Peaks Over Threshold (POT) method. Then, extreme spatial events were defined by finding simultaneous high-water levels that affected at least four tide gauges within a storm window of 3.5 days. To broaden the understanding of the spatial footprints of storm surges for the global coastline, Enríquez et al. (2020) assessed the spatial patterns of storm surges using tide gauge observations and a high-resolution storm surge reanalysis. In this global analysis, they first divided the coastline into segments according to the similarity among storm surge time series using a K-means algorithm. For each cluster, a "reference series" was defined and assumed to be representative of each region; the reference series was then used to apply a match level analysis and copula analysis to obtain the spatial footprints in terms of co-occurrences and joint return periods. This global approach highlighted those coastline stretches more likely to be impacted simultaneously by the same storm surge events. Large-scale footprints that affect several regions or states/countries and even unconnected coastline stretches were detected. Comparing the global and regional studies shows, for example, that while four spatial patterns of skew surge footprints were found in the regional study along the UK coastline (Haigh et al., 2016), and two patterns were detected along the NZ coastline (Stephens et al., 2020), these were simplified to three types for the UK and one for NZ in the global scale analysis (Enríquez et al., 2020). This discrepancy highlights that although global studies are valuable because they provide an overall picture of areas with higher spatial dependence in surge events, there are relevant local features which may not be fully captured at this scale.

The aim of this paper is therefore to undertake a deeper comprehensive investigation of the spatial dependence during extreme storm surge events within a specific regional area, by developing and applying a novel spatial tracking approach. We analyse independently only the meteorological component generated by atmospheric pressure and wind stress (the waves are not considered). To achieve our objective, we consider the UK and Irish coastlines (similar to Haigh et al., 2016) but rather than using measured tide gauge data we consider outputs from a high-resolution sea level hindcast (the Coastal Dataset for the Evaluation of Climate Impact, CoDEC; Muis et al., 2020) which provides a homogenous spatio-temporal mapping of non-tidal residual data around the UK and Ireland for the period 1980 to 2017. First, our novel approach (Fig. 1) involves the development of a new tracking algorithm to identify multi-site storm surge events around the UK and Ireland over the hindcast period 1980 to 2017. Second, each spatial event identified is defined by its duration, footprint and severity based on the return period reached along the coast during each event. This characterization facilitates the analysis of the spatial distribution and interannual variability of the spatial event collection. Third, we classify each of the individual surge events into types, using the k-means algorithm, to distinguish patterns of surge footprints that represent coastal stretches that are prone to being simultaneously impacted by storm surges of the UK and Irish coasts. Fourth, we apply a storm tracking algorithm to the same atmospheric forcing (i.e., sea level pressure and wind from ERA5) used to derive the modelled storm surge to extract the tracks of the storms responsible for each distinct spatial extreme storm surge event we identify.

The paper is organised as follows: data and methods are described in detail in sections 2 and 3, respectively. The application of the four steps in which the general framework has been divided, with the corresponding outputs, is contained in section 4. The results are summarised and discussed in section 5, and main conclusions are outlined in section
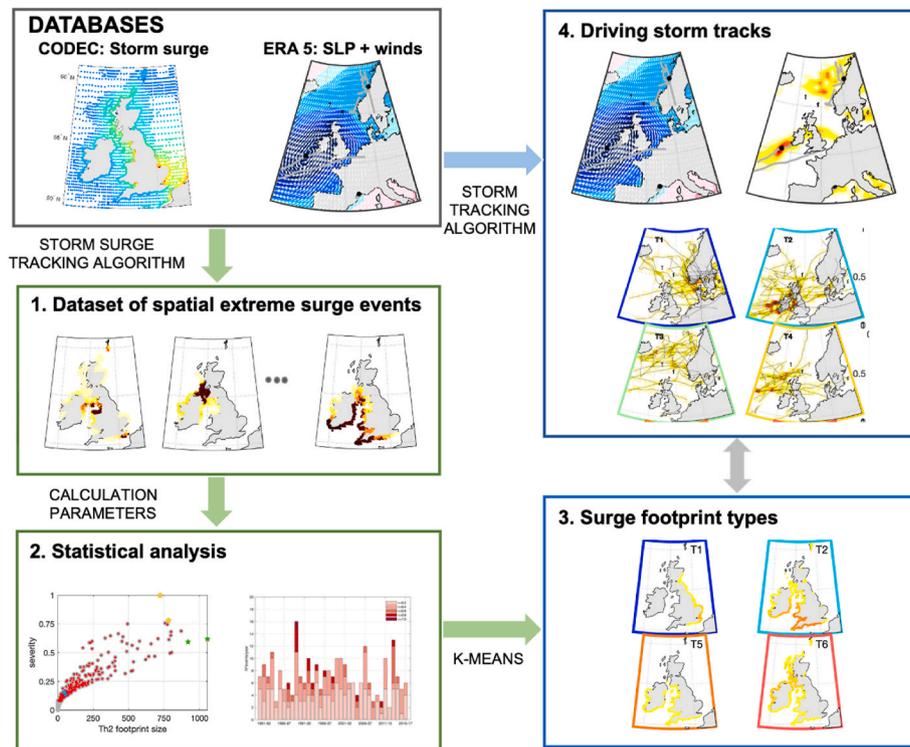
Fig. 1. Illustration of the datasets used, methods applied and the four main steps of the methodology.

6.

2. Data

In this study, we use two sources of data, namely hindcast storm surge time series and meteorological reanalysis fields. These two datasets are described below.

2.1. Storm surge

First, we use storm surge outputs from a hindcast database to characterize the spatial footprint of storm surges around the UK and Ireland. Hourly modelled storm surge time series have been extracted from the Coastal Dataset for the Evaluation of Climate Impact (CoDEC) (Muis et al., 2020) reanalysis, which is publicly available on the Copernicus Climate Change Service (C3S) Climate Data Store (https://cds.climate.copernicus.eu/cdsapp#!/dataset/sis-water-level-change-timeseries?tab=overview). The third generation Global Tide and Surge Model (GTSM, Kernkamp et al., 2011), with a coastal resolution of 1.25 km in Europe, was forced with meteorological fields from the ERA5 climate reanalysis to simulate extreme sea levels. Tides are induced in the model by incorporating tide generating forces using a set of 60 frequencies. Therefore, interaction effects between tides and surge are included. A tide-only simulation is carried out to break down the total water levels into the different sea level components. Afterwards, the surge level time series are calculated by subtracting the tides (i.e., tide-only simulation) from the total sea level. These surge levels should be called non-tidal residuals, which is a more accurate term (Arns et al., 1918). However, for simplicity, we refer to them as storm surge throughout the text. The effect of the waves is absent from this database as its inclusion would require coupling a hydrodynamic and wave model on a global scale. As a results, there is no wave setup. The influence of the waves on the wind stress, usually considered via a varying drag coefficient, is also not accounted for. In fact, a constant drag coefficient of 0.0041 is used to estimate the wind stress at the ocean surface (Muis et al., 2020).

The study domain and location of each of the CoDEC model grid point are displayed in Fig. 2. The domain extends from latitude 49°–61° and longitude −12°–4°. Over this domain, time series of storm surges between 1980 and 2017 are gathered at 2,962 grid points, out of which are 1,335 coastal grid points. The resolution of the output GTSMv3.0 grid points changes, starting from 0.1° at the coast, to 0.25° within 100 km of the coast, and 0.5° at 500 km or greater distance from the coastline. Fig. 2a shows the spatial distribution of the 99.9th percentile of the surge for the period 1980–2017, highlighting larger storm surges in the shallow and funnelled stretches of coastline of the Bristol Channel, eastern Irish Sea and southern North Sea.

We conducted a validation of the CODEC hindcast using all available tide gauges situated around the UK, previously utilized in studies such as Haigh et al. (2016) or Hendry et al. (2019). Error metrics, including the root mean square error (RMSE) for surges over the 99th percentile and Pearson's correlation coefficient, were computed for 41 tide gauges. Spatially plotted error metrics, along with differences in the 95th and 99th percentile of CoDEC and tide gauge surges, are presented in the Supplementary Data. Additionally, comparisons of time series and scatter plots at two tide gauges are provided as examples. The results indicate good performance of the CODEC hindcast in the study area, with mean RMSE and correlation coefficients in the range of 0.1–0.2 m and 0.8–0.9, respectively. Areas exhibiting less accurate simulation of non-tidal residuals align with the Bristol Channel, suggesting a potential need for higher-resolution bathymetry and consideration of river interactions. Notably, the tracking algorithm and classification are based on the spatial evolution of surges rather than specific values at individual locations. Whilst discrepancies in surge magnitude exist, they are not expected to significantly impact the values of return periods and, consequently, the severity index. Futhermore, any potential impact would be confined to small surge events in the Bristol Channel, which is beyond the scope of our study.

2.2. Atmospheric conditions

Secondly, we utilize meteorological fields from a reanalysis to extract storm tracks that impact the UK and are accountable for the
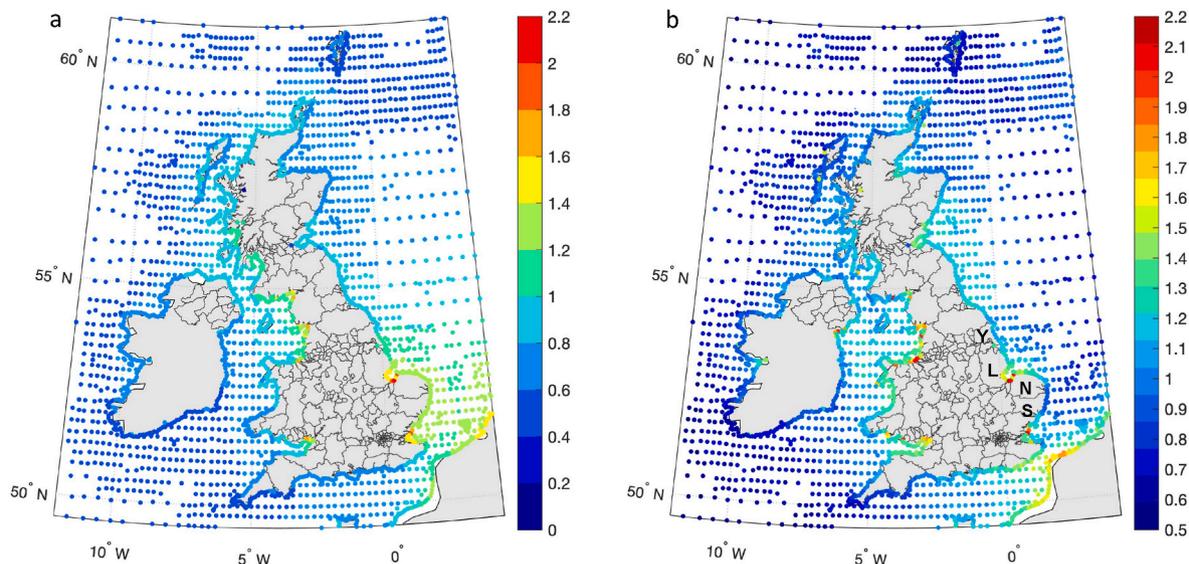
Fig. 2. (a) Spatial distribution of the 99.9th percentile of the surge, in m, along UK and Ireland coastlines; (b) Number of events per year selected by POT for the 99.9th percentile as the threshold.

extreme spatial storm surge events we identify. Hourly sea level pressure (SLP) and wind fields are extracted from the ERA5 reanalysis (Hersbach et al., 2020) on a regular latitude-longitude grid at 0.25° × 0.25° resolution. We deliberately chose to use the ERA5 reanalysis, as opposed to other available meteorological reanalyses, because the CoDEC database was created using ERA5. The ERA5 hourly dataset spans 1940 onwards and it is currently publicly available at the Copernicus Climate Change Service (https://cds.climate.copernicus.eu/cdsapp#!/dataset/reanalysis-era5-single-levels?tab=overview). The reanalysis combines model data with observations into a globally complete and consistent dataset using the laws of physics.

3. Methods

Our approach includes for main stages to obtain and analyse the spatial footprints of storm surges: i) a storm surge tracking algorithm, ii) calculation of three parameters for each spatial event, iii) the K-means technique, and iv) a storm tracking algorithm. Firstly, we develop and apply a new approach based on the concept of a tracking algorithm to identify multi-site storm surge events around the UK and Ireland over the hindcast period from 1980 to 2017. Second, we create several parameters to summarize the characteristics of the spatial extreme surge events detected, with the severity index being the most novel. Third, the K-means is used to cluster the spatial extreme events into types to assess the different coastal stretches impacted. Fourth, the storm tracking algorithm is applied to extract the extratropical storm tracks that cross the Atlantic Ocean near or over the UK and Ireland during throughout the surge hindcast period. The aim is to link each unique spatial extreme surge event with the corresponding responsible storm.

3.1. Storm surge tracking algorithm

A new tracking algorithm approach is applied to the CoDEC storm surge hindcast around the UK and Ireland to distinguish distinct spatial storm surge events that have occurred over the 38-year period 1980 to 2017. We develop a simplified version of a commonly used Lagrangian tracking algorithm of pointwise features (such as cyclones and eddies; Ullrich and Zarzycki, 2017) with the objective of identifying and tracking sea surface features, in this case footprints of storm surges.

Before applying the track algorithm, we perform a preprocessing of the CoDEC surge time series. The preprocessing is carried out separately at each of the 2,962 CoDEC grid points in our study area. Firstly, we

calculate the maximum storm surge every 3 h to reduce the computational time of the algorithm. We also identify independent peaks by applying a Peak Over Threshold (POT) approach to each 3-hourly time series. To ensure independent peaks, we decluster the time series considering a storm window length of 3 days. The 3-day storm length has been used in previous studies (e.g., Haigh et al., 2016; Camus et al., 2021) and equates to the typical time it takes for a storm to approach and cross the UK and Ireland. Here, we use the 99.9th percentile as the POT threshold to limit our analysis to the most extreme storm surge events (a sensitivity analysis of TH1 and TH2 thresholds in the identification of spatial extreme surges is provided in Supplementary Data).

The surge tracking algorithm consists of connecting the spatial footprints of storm surges through time and space that define a spatial surge event. 3-hourly spatial footprints of storm surges are defined as the model points that simultaneously exceed threshold 1 (hereafter referred to this as TH1; we use the 95th percentile in this study) and at least one model grid point also corresponds with a declustered peak above threshold 2 (hereafter referred to as TH2; we use the 99.9th percentile in this study) for each time step. Spatial footprints are only considered to be part of the same event if the coastal centroid of the footprint (the average position of the coastal grids with a surge that exceeded the TH1 threshold) in the subsequent time step is less than 6° (tracking distance) from the coastal central point of the surge footprint in the time step before. We tested different tracking distance thresholds, and visual inspection of each distinct event with the corresponding storm tracks showed that 6° worked well at isolating and separating different spatial events that occurred close together in time. At this stage we end up with 536 distinct spatial events, each with a specified duration.

3.2. Calculation of parameters for each spatial extreme surge event

We consider three parameters, i.e., duration, size and severity, to characterize each spatial extreme surge event. The duration of each event is determined by the number of 3-hourly footprints concatenated. We define the footprint size as the count of coastal grid points where the surge exceeds the TH2 threshold (i.e., 99.9th percentile) during the duration of the event. The CODEC outputs are presumed to be available at 10 km intervals along the European coastline, with equidistant sampling applied to the smoothed Natural Earth 1:10 coastline (Muis et al., 2020). Therefore, we infer that 1335 coastal grid nodes along the UK and Ireland coastline equate to 13,340 km. To standardize the size of each
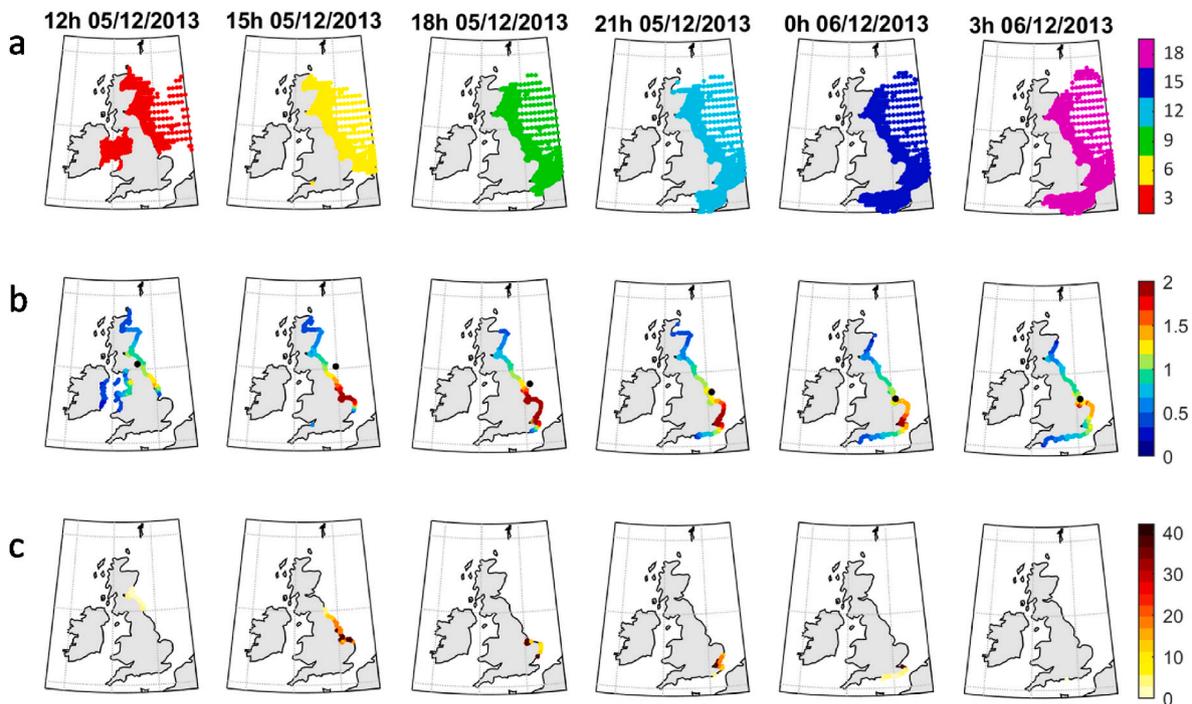
Fig. 3. Surge tracking algorithm for a surge event which started on the December 5, 2013 at 12 h and finished on the December 6, 2013 at 3 h: (a) Spatial footprints every 3 h (sites with a surge over the TH1 threshold equal to the 95th percentile) for a total duration of 18 h; (b) Surge value, in m, at coastal sites that constitute each footprint and the coastal centroid of the footprints (black circle); and (c) Empirical return period, in years, of surge at coastal sites of each footprint where a POT event over the TH2 threshold (99.9th percentile) occurred.

spatial surge event, we convert the number of coastal grids to kilometers of coastline using this conversion, expressing the size in a uniform unit (kms).

Event severity is estimated by means of an index derived from the combination of the empirical return period of the surge levels (peaks over the TH2 threshold, 99.9th percentile) and the footprint size for each of the spatial surge events identified. The corresponding empirical return period to each peak at each grid node is calculated. Empirical return periods are assigned to observed extreme values using an empirical rule where extreme values are ordered and ranked from the most extreme (1) to the least extreme (N), then exceedance probabilities are calculated as:

$$p = \frac{r}{N+1}$$

where r is the rank of extreme value (1 to N), and N is the number of extreme values. Empirical return periods are calculated as:

$$ERT = \frac{\lambda}{p}$$

where λ is the rate of extreme events (average number of extreme events per year) calculated as the number of extreme events within the total duration (in years) of series from which the extreme values were drawn.

For each event, we sum the empirical return periods to create a single number, which essentially takes into account the overall extremeness of a particular event. These values are normalised between 0 and 1 and scaled by a cube root so that the distribution of the highest severity index values varies more linearly.

3.3. Classification algorithm

We classify the spatial extreme surge events identified using the proposed methodology into several types by applying the k-means algorithm to the maximum value of the storm surge during each spatial event. Therefore, each datum is defined by a surge value at each grid

node of the study domain (2,962). Principal component analysis is used to reduce the dimensionality of the data, with only 6 principal components needed to explain the 95% of the variance. To define a typology, we use a version of the k-means algorithm that initiates the clusters using the maximum-dissimilarity algorithm, guaranteeing the most representative initial subset and a deterministic classification (Camus et al., 2014). Several numbers of clusters (from 6 to 16) were tested, observing the subdivision process of some of the clusters as the number increases. The 8 clusters provide the most accurate representation of the spatial distribution patterns of extreme surge levels along the UK and Ireland coast, delineating the coastal stretches most likely to experience surge impact.

3.4. Storm tracking algorithm

We use the storm track identification software developed for application to storms on the East Coast of the US (HR Wallingford/USACE, 2022) to extract and analyse the extratropical storm tracks that cross the Atlantic Ocean near or over the UK and Ireland during our study period (1980–2017). We use the ERA5 atmospheric reanalysis historical 2D horizontal spatial sea level pressure and u and v wind speed fields at 10 m elevation. The storm tracking algorithm comprises of two steps, namely: (1) detection and (2) tracking. Firstly, the detection step revolves around a vortex strength algorithm which was originally defined by Graftieaux et al. (2001) and later modified by Endrikat, and subsequently Zigunov. The vortex strength is calculated according to the 2D convolution of the u and v wind components. To detect potential significant storms, a threshold, G1, for vortex strength is applied. Specifically, for each hour between 1980 and 2017, we identify the grid cells where the vortex strength exceeds 0.5. We note that G1 value's range is between −1 and 1 and, therefore, a value above 0.5 captures relatively low-intensity cyclonic wind patterns. An additional pressure threshold (1010 mbar) is used to filter out low-intensity storm events. For each ERA5 hour where the threshold is exceeded, we record the latitude and longitude of the grid cell with the maximum vortex. This corresponds to

the centre of the storm, at a given time. Second, the tracking step consists of following distinct storms across subsequent time steps. This is done by applying a nearest neighbour detection approach with a maximum distance threshold of 5°. The final output is a set of potentially significant storms. For each distinct storm we record, at hourly intervals, the time, the location of the centre of vortex (G1>0.5), the vortex area exceeding the G1 threshold, the maximum vortex value in that area, the minimum air pressure within the G1 area, the area below a pressure threshold of 1010 mbar around the vortex centre and mean and maximum wind speed in the pressure exceedance area.

4. Results

Firstly, the performance of the tracking algorithm in identifying spatial extreme events is shown. Secondly, the characteristics of each event are assessed in terms of duration, size and severity, facilitating an evaluation of their spatial distribution and temporal variability. Thirdly, the K-means algorithm is employed to identify areas most prone to be impacted by these spatial events. Fourthly, each spatial event is linked with its respective storm track, and an analysis of the storm characteristics is conducted based on surge footprint clusters.

4.1. Construction of a dataset of spatial extreme surge events

Fig. 3 shows the spatial footprints for a notable storm surge that occurred on 5th and December 6, 2013, produced by cyclone Xaver, that resulted in some of the most significant coastal flooding in the last 60 years. Fig. 3a shows the CoDEC points that exceed TH1 (95th percentile) every 3 h over the 18-h duration of the event, illustrating the changing event footprint over time. Fig. 3b shows the maximum 3-hourly surge levels (in meters) over the event, for the coastal grid points. Fig. 3c shows the empirical return periods (in years) of the coastal grid points that exceed TH2. The spatial extent and movement of the storm surge

are consistent with results from previous studies that analysed this exceptional event (e.g., Spencer et al., 2015; Wadey et al., 2015; Haigh et al., 2016), demonstrating the tracking model's ability to follow the evolution of the spatial footprints of storm surges along the coast. At the start of the event, at 12:00 on the December 5, 2013, surge levels were elevated in the Irish Sea and then along the northern part of the UK East coast. Over the duration of the event, the storm surge propagated down the UK East coast and into the English Channel. The empirical return periods of the event were highest along the coastline of the counties of Yorkshire, Lincolnshire and Norfolk (marked with a Y, L and N in Fig. 2).

Many of the identified events may have very small footprints, short duration, and low severity. Because our main interest is to analyse the most extreme and larger footprints, we reduce the number of events by eliminating those with low severity. A severity index lower than 0.075 was chosen to restrict the final number of events to around 300 (from 536 to 270) for the most extreme events and, therefore, those with the greatest potential for coastal impact. This equates to an average of ~approximately 7 events per year. Note that this number of events refers to all the spatial surge events detected along the UK coastline and cannot be compared with the number of extreme surges at each location shown in Fig. 2b.

4.2. Statistical analysis of the spatial extreme surge events

In Fig. 4, we can observe a linear relationship between severity and footprint size (a Pearson's correlation coefficient of 0.88 with a p-value lower than a significant level of 0.05), as anticipated, owing to the definition of the severity index that is founded on the value of the return period at all points specifying each individual surge event. However, if we examine the occurrences with a severity index above 0.5 (30 events), we can discern that their sizes practically encompass the range of potential values (with a minimum of approximately 2,000 km up to 10,000 km). This implies that for those highly severe spatial extreme surge
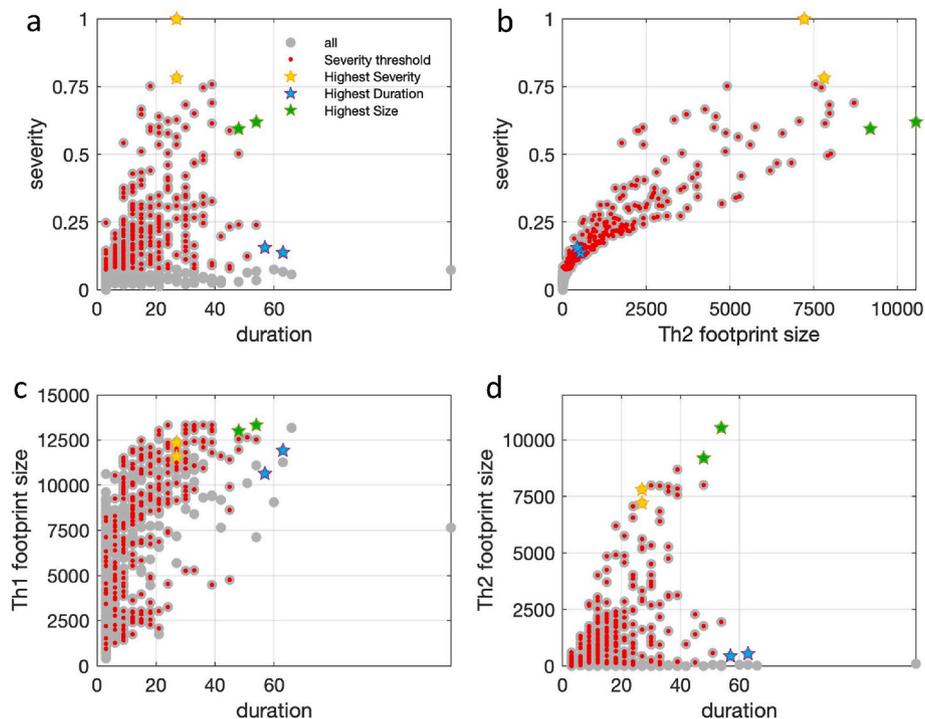

Fig. 4. a) Duration, in hours, vs severity index (values between 0 and 1); b) TH2 footprint size (km of coastline where surge exceeded the TH2 threshold equal to 99.9th percentile) vs severity index; c) Duration, in hours, vs TH1 threshold footprint size (km of coastline where surge exceeded the TH1 threshold equal to 95th percentile); d) Duration, in hours, vs TH2 footprint size of the collection of extreme surge events (in grey: all events; in red: after eliminating those events with a severity index lower than 0.075). Starts represent the two surge events with the highest severity (yellow), with the highest duration (blue) and with the highest size (green).

events with small size, the impact is restricted to a limited coastal stretch. Note that footprint sizes can cover the entire coastline of our study domain, which corresponds to 13,340 km (one grid node every 10 km).

On the other hand, there is a greater dispersion between the severity and the duration of the events (correlation coefficient of 0.41). In fact, we can observe a certain polarization in this relationship, with events of maximum duration and maximum size (relative to Th2 threshold), and events of maximum duration and small size. We can observe that the two events with the longest durations selected from the final subset, shown in Fig. 5c and d, present high Th1 size but very low Th2 size with surge values corresponding to low return periods, resulting in low severity. In any case, the durations are close to the two events with the largest sizes.

The dates of the 20 highest severity events are listed in Table 1. The events with the two highest severity indices are shown in Fig. 5a and b, the two longest events are shown in Fig. 5c and d and the two largest events are shown in Fig. 5e and f. In each panel of these figures, the left subplot shows the CoDEC grid points with a surge above TH1 (i.e., 95th percentile), coloured by the corresponding 3-hourly time step. The right subplot displays only the coastal points where the surge is above TH2 (i. e., 99.9th percentile), coloured by the magnitude of the empirical return period. These six examples show events that lasted between 18 and 63 h, with spatial footprints that impacted different stretches of the UK coastline. The events with the two highest sizes correspond to the 14th and 19th most severe events, respectively, while they are the third and sixth events, sorted by the footprint size. This correspondence is due to the linear relationship observed above between the severity and the footprint size. In the case of the longest events, the area in which surge values above the Th2 threshold are reached is small, which is reflected in a severity of the order of 0.15 in both cases.

Once the extreme spatial surge events have been identified and synthesized using the parameters severity, duration and size, their spatial distribution along the study coast can be analysed. For this purpose, the number of events that pass through each coastal location and the mean value of the three parameters are calculated (see Fig. 6). This spatial characterization of the events allows us to identify the coastal areas most prone to extreme surge events and their severity, duration and mean size. Regarding the number of events impacting each coastal location (Fig. 6a), the most affected coastal stretches are concentrated on the northern coasts of the Irish Sea, and large estuaries that flow into the North Sea, such as the Thames (London), the Wash (between the counties of Lincolnshire and Norfolk, L and N in Fig. 6b) or the River Forth (Scotland, F in Fig. 6b), with about 60 events during the study period (1980–2017), while in the rest of the study area the number of events was around 30. The coastal configuration (coastal inlets) contributes to the amplification of the surge generated by storms.

A gradient from northwest to southeast can be observed in the mean duration, footprint sizes and severity of extreme events. The similarity in the spatial distribution of the three parameters characterising the surge events is due to the linear relationship found between them (Fig. 4). Durations are of the order of 30 h on the coasts of Northern Ireland and Scotland, dropping to durations of the order of 24 h on the west and east coast of the UK to values of the order of 18 h in the south of England and Ireland (Fig. 6b). In the case of the size (Fig. 6c), the largest footprints occur in the northwest of the study area (north and east of Ireland, west of Scotland), while the smallest occur in the southwest of England (Cornwall, C in Fig. 6b) and southeast of England (including Suffolk and Norfolk, S and N in Fig. 6b). The mildest spatial events (of the order of 0.2) are more likely to occur around the Thames Estuary area in terms of severity (Fig. 6d).

The temporal variability of the spatial extreme surge events by season is analysed, sorted by the severity index (Fig. 7). We define a season as covering the period from July in one year to June in the following year, to encompass the storm surge winter period. In terms of the
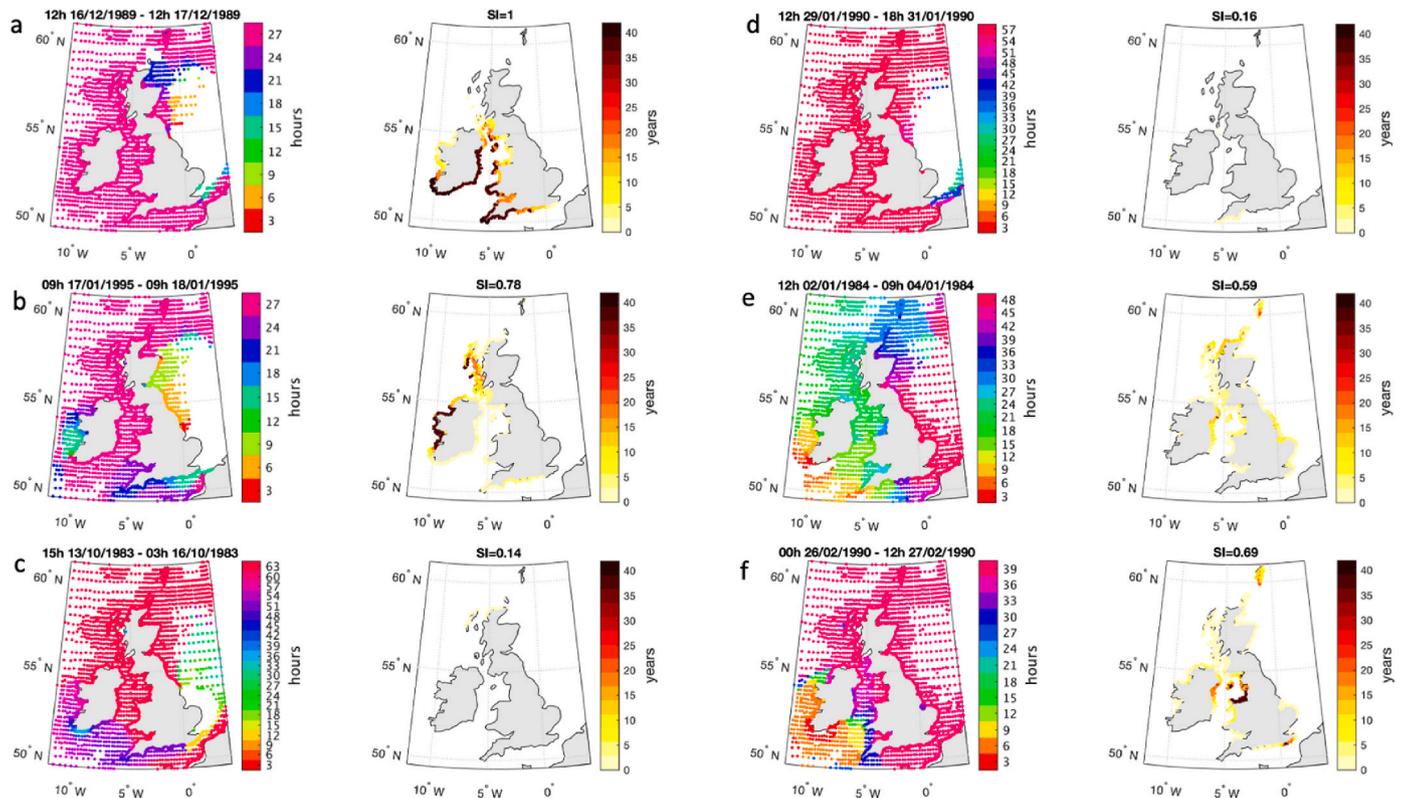

Fig. 5. The two most severe storm surge events based on the severity index (a and b), the two longest storm surge events (c and d) and the two largest events (e and f). Left panel of each event shows the 3-hourly spatial footprints that constitute the surge event (locations with a surge over the TH1 threshold equal to 95th percentile). Right panel shows the empirical return period of surge, in years, at coastal sites of all the footprint sites where a POT event over the TH2 threshold (99.9th percentile) occur, with the value of the severity index (SI).

Table 1
The top 20 events based on severity index (values from 0 to 1), duration (hours) and TH2 footprint size (kms of coastline with a surge value over TH2 threshold equal to 95th percentile).

20 MOST SEVERE				20 HIGHEST DURATION				20 HIGHEST TH2 FOOTPRINT SIZE			
DATE	SEVERITY	DURATION	TH2 SIZE	DATE	SEVERITY	DURATION	TH2 SIZE	DATE	SEVERITY	DURATION	TH2 SIZE
16/12/89 12:00	1,00	27	7210	13/10/83 15:00	0,14	63	530	30/3/94 9:00	0,62	54	10,550
17/1/95 9:00	0,78	27	7810	29/1/90 12:00	0,16	57	440	2/1/84 12:00	0,59	48	9190
11/1/05 9:00	0,76	39	7560	30/3/94 9:00	0,62	54	10,550	26/2/90 0:00	0,69	39	8700
26/12/98 12:00	0,75	18	4910	23/2/97 6:00	0,24	54	1930	1/2/02 3:00	0,50	48	8020
16/1/93 21:00	0,75	36	7730	28/1/13 9:00	0,12	51	570	19/2/90 3:00	0,68	30	7980
26/2/90 0:00	0,69	39	8700	2/1/84 12:00	0,59	48	9190	19/2/97 9:00	0,65	33	7970
19/2/90 3:00	0,68	30	7980	25/12/90 6:00	0,24	48	1760	2/12/06 21:00	0,49	36	7920
25/1/90 3:00	0,67	15	4260	1/2/02 3:00	0,50	48	8020	10/1/93 9:00	0,61	39	7840
19/2/97 9:00	0,65	33	7970	14/2/89 0:00	0,59	45	2280	17/1/95 9:00	0,78	27	7810
12/2/14 9:00	0,65	15	3700	19/9/90 3:00	0,09	45	160	16/1/93 21:00	0,75	36	7730
9/2/88 3:00	0,64	21	4580	21/2/02 0:00	0,08	45	160	11/1/05 9:00	0,76	39	7560
3/2/11 15:00	0,63	27	3330	23/12/13 12:00	0,23	45	1390	16/12/89 12:00	1,00	27	7210
1/2/90 12:00	0,62	24	7070	8/1/91 12:00	0,20	42	950	1/2/90 12:00	0,62	24	7070
30/3/94 9:00	0,62	54	10,550	12/2/82 15:00	0,33	39	3130	17/1/09 12:00	0,47	33	6840
10/1/93 9:00	0,61	39	7840	26/2/90 0:00	0,69	39	8700	14/1/15 18:00	0,58	24	6570
26/12/13 18:00	0,60	21	5760	10/1/93 9:00	0,61	39	7840	9/11/98 0:00	0,47	33	6410
5/12/13 12:00	0,60	18	2400	29/11/00 3:00	0,09	39	170	8/2/14 0:00	0,44	18	6200
4/2/14 15:00	0,60	30	4520	11/1/05 9:00	0,76	39	7560	26/12/13 18:00	0,60	21	5760
2/1/84 12:00	0,59	48	9190	25/12/16 18:00	0,10	39	200	28/1/02 3:00	0,54	27	5610
14/2/89 0:00	0,59	45	2280	19/12/82 9:00	0,34	36	5280	31/1/88 18:00	0,42	30	5330

number of events per season, 1989–90 emerges with 16 events, followed by 2013-14 with 13 events and 2006–07 with 12 events. If, in addition to the number of events, the severity is considered, 1989–90 and 2013–14, stand out for their extremity. The most severe event occurred in 1989-90, which also had 4 other events with a severity of between 0.8 and 0.6. For the 2013-14 season, there was one event with a severity in this range and 6 other events with a severity between 0.4 and 0.6.

4.3. Surge footprint types

The 8 footprint types were derived by applying the k-means algorithm to the dataset comprising 270 spatial storm surge events. Each event is characterized by the maximum surge value attained throughout its duration. Subsequently, for the representation of each cluster, we defined each event based on the return period corresponding to every surge peak above the TH2 threshold. The graphical representation of each footprint type was achieved by calculating the average return period of all events associated with each cluster. This approach enables us to highlight the coastal stretch where the surge impact is concentrated for each footprint type (see Fig. 8).

Each type is framed in a colour, which has been used for the subsequent representations of the corresponding surge event characteristics associated with each type, and the corresponding storm tracks of each individual event (Section 4.4). For each of the 8 footprint types, Fig. 9a shows box plots representing the range of the corresponding severity, duration (in hours) and footprint size (number of coastal sites with a surge value over the TH2 threshold). Each box plot shows the 25th and the 75th percentile range of that variable, and individual markers above and below the box represent the maximum and the minimum of these variables. The bottom panel in Fig. 9a shows the number of events

corresponding to each classification footprint type.

Based on the return periods of the types, the most notable types are T2 (cyan), T3 (green) and T7 (magenta), which show a concentration of the impact in the southwest of the UK, east coast of the UK, and the north coast of Scotland, respectively. If we look at the characteristics of these events (Fig. 8a), we can observe that they present the highest values of severity, duration and size, especially T7. It should be noted that the individual event with the highest severity (16th-17th December 1989) is represented by T2 due to its similarity in the spatial pattern of return periods, but due to its severity it can be considered almost an outlier. The most frequent T6 (red), which hits the north coast of Ireland and the northern part of the Irish Sea, also has similar ranges of severity and duration to T2 and T3. However, T6 characterises events with a larger footprint than these two types, which explains why the corresponding return periods of the storm surge are lower at each individual location, despite a similar severity value (see Fig. 9).

The remaining types can be considered as T2, T3 and T6 variations. Types T1 (blue) and T8 (purple) represent events affecting the east coast of the UK, with a greater concentration of impact to the south and north, respectively, but of less significance in terms of severity, duration and size than T3. Types T4 (yellow) and T5 (orange) types can be considered as light versions of T6 and T2 respectively in all their characteristics.

The number of events per season, for each of the 8 types, is shown in Fig. 9b. There is considerable variability between seasons. In the two seasons with the highest number of events overall, 1989–90 and 2013–14, we can see that spatial surge events affecting the south-east coast of the UK (T1) only occur in 2013–2014, whereas in 1989-90, events affecting the northern part of the study area (T7 and T8) were more frequent.
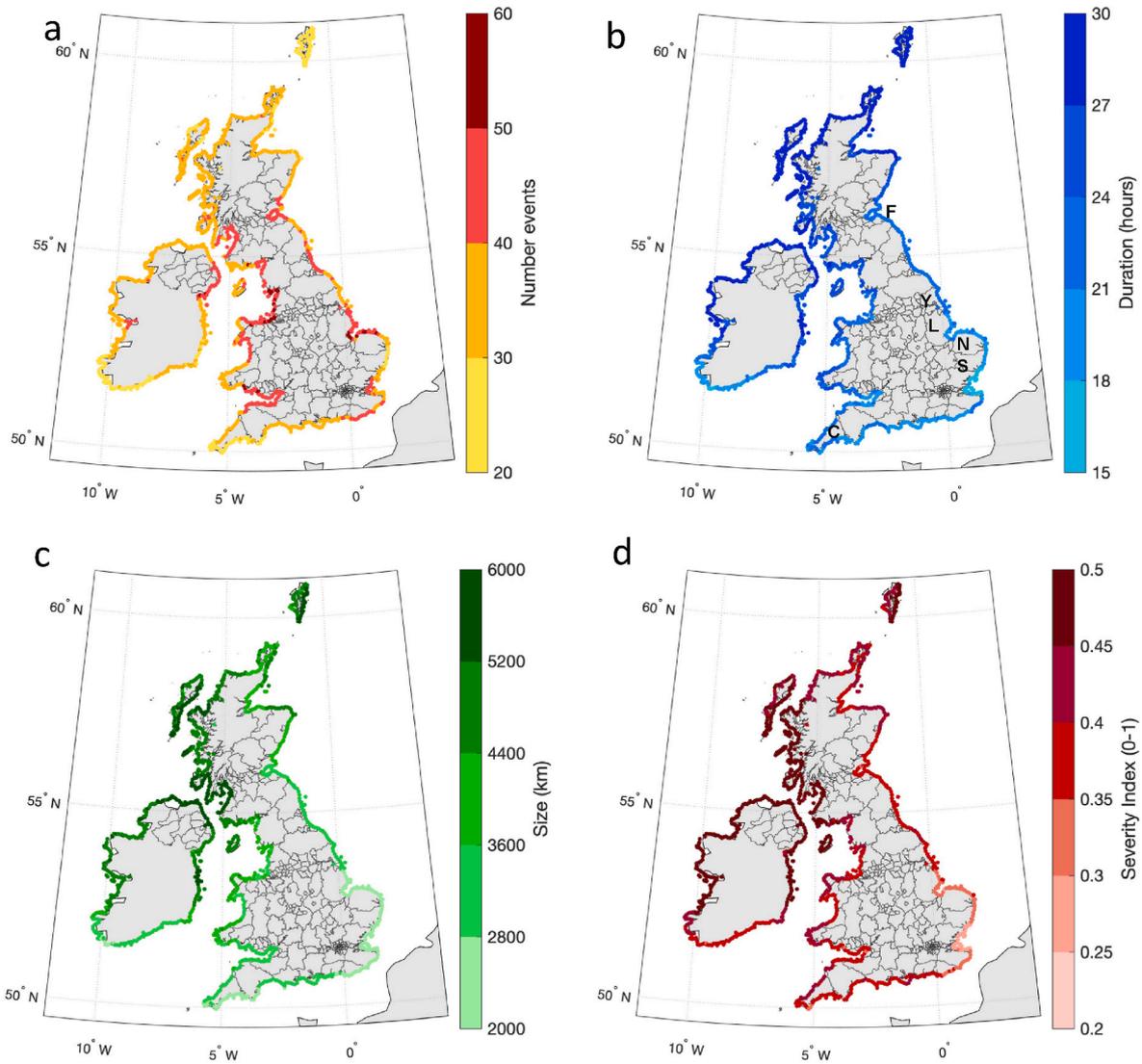
Fig. 6. Spatial characterization of the collection of 270 surge events: (a) number of events; (b) mean duration (in hours), (c) mean TH2 footprint size (in km of coastline where the surge level exceeded the TH2 threshold) and (d) mean value of the severity index (range value between 0 and 1) of all events that pass through each coastal site.
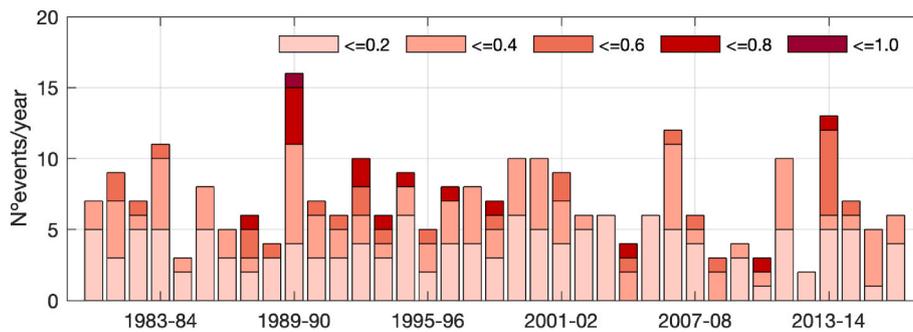

Fig. 7. Number of extreme spatial surge events between 1980 and 2017, categorized according to their severity index values ranging from 0 to 1.

4.4. Driving storms

For each of the 270 distinct spatial extreme surge events, we identify the closest storm track from the output database at that time. From each storm, we consider a number of variables that characterize its main physical attributes. We identify the minimum pressure (P_{min}) of the track segments that coincide in time with the surge events. We consider the corresponding P_{min} as a measure of the intensity of the track and the area below the pressure threshold (1010 mbar) as a measure of the range of action. We calculate the forward speed, derived from successive storm coordinates for the coincident segment, as an indicator of the impact on the coast in relation to surge (units are km/hour). It has been shown, at
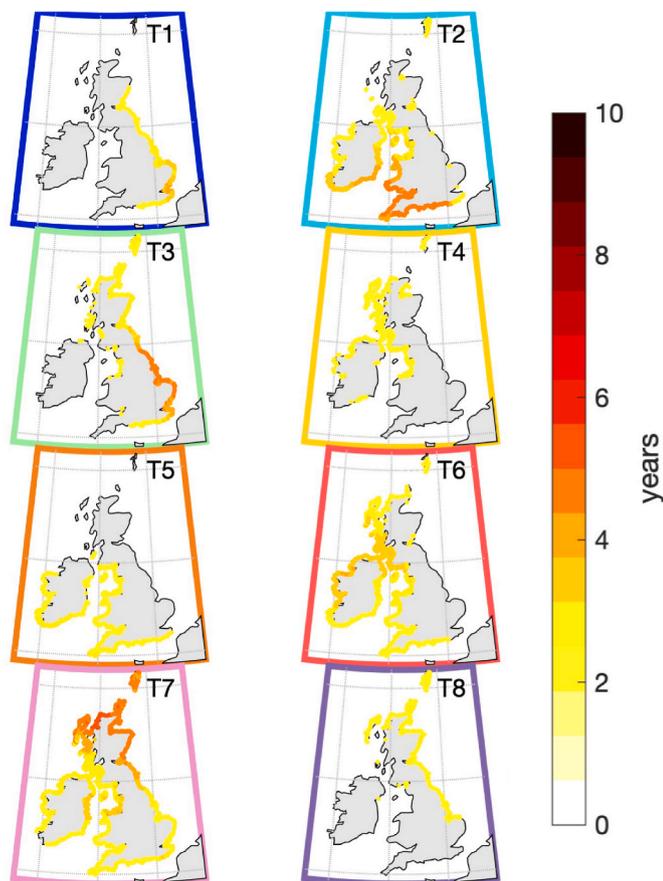
Fig. 8. Surge footprint types represented by the spatial distribution of the average return period of non-tidal residuals of the surge events within each cluster.

least for tropical cyclones, that slow-moving storms have more time to collect and push water around to generate deeper and more impactful storm surges (Thomas et al., 2019). We also calculate the mean distance between the coincident track segments and the centroid of the surge footprint as another measure of the action radius of the storm track.

The tracks of the storms that correspond with each of the extreme spatial surge events are shown in Fig. 10, for each of the 8 footprint types, along with storm density per $1.0° \times 1.0°$ degree grid cell. Although there is overlap and spread, the typical tracks of the storms are somewhat distinct for each spatial type. For each of the 8 types, the range in four key storm characteristics is shown in Fig. 11. We observe slight differences between the 25th and 75th percentile ranges of the parameters, the more notable being that storms passing over higher latitudes have lower P_{min} and higher area $P < 1010$ mbar (Types 6, 7 and 8) (Fig. 11a).

The location and orientation of the storm tracks associated with each event and within each footprint type explain the different spatial patterns of the impacted coastal stretches (represented by return period values). The most evident case is presented for the events impacting the east coast of the UK. In the case of T1 (blue), whose zone of impact is the southeast of the UK, they are generated by storms located to the east of the UK, with a predominant north-south direction. In the case of T3 (green), whose impact zone covers a larger area, storms occur at higher latitudes, above the study area, with a west-east orientation and a further eastern action area, while for T8 (purple), with an impact extending from the north to the middle of the east coast of the UK, the events are produced by storm tracks with a southwest-northeast orientation. If we look at the characteristics of the storms, in terms of Pmin and AreaPmin, the storm tracks associated with T1 are of lower

intensity, which would explain the smaller footprint size. On the other hand, the tracks pass closer to the coast and with a lower translation speed, which would be consistent with a more localised effect of the surge.

The rest of the footprint types are associated with tracks generated in the North Atlantic with a southwest-northeast direction, mainly, and the impact concentration zone is determined by the latitude of the track's passage or its proximity to the coast. The most intense tracks (Pmin) are those corresponding to T7, which are in turn associated with the most severe surge events with the greatest extent and duration.

We find that among the four parameters characterizing each storm track (P_{min}, Area with $P < 1010$ mbar, Forward Velocity and Distance), only the Pmin exhibits a certain linear relationship with the severity, footprint size and duration of each spatial surge event. Scatter plots presented in Supplementary Figure SM5 depict the relationships between the key storm characteristics and the surge event attributes within each cluster. The linear relationship between the parameters of the storms and surge events is represented by the line of best fit, displaying a clear negative relation with Pmin for clusters that contain the more intense atmospheric storms (lower Pmin). Only regression slopes that are statistically different from zero are shown. This implies that the p-values associated with the t-tests for the regression coefficients are smaller than the 0.05 significance level, indicating a statistically significant relationship.

5. Discussion

In this study, we employed a novel tracking algorithm on a storm surge hindcast to identify spatial extreme surge events along the coastlines of the UK and Ireland. Initially, we identified a total of 536 spatial surge events from the storm surge hindcast spanning the period from 1980 to 2017. Each surge event captured was characterized by its duration, footprint size and severity, assessed based on the return period. To focus on the most spatially extreme events, we applied a severity index threshold, resulting in a final dataset of 270 events. The event sample has been classified into 8 surge footprint types based on their spatial extent around the coastline. We have analysed the spatial distribution and the interannual variability of the characteristics of the surge events and linked them with their driving storm tracks and characteristics. The novel framework we have developed could easily be extended to other coastal locations around the world and could even be carried out on a global scale. Note that in this paper our analysis focuses only on the storm surge component of sea level, in fact the non-tidal residual provided by CODEC, as this is directly related to a storm. We ignore the astronomical tidal component, and hence the total extreme sea levels that ultimately determine the extent of coastal flooding. However, the approach developed here could easily be extended to the other drivers of the total water level, i.e., waves, or even to the total water level itself in the future.

In the following we qualitatively compare our results with the spatial analysis of tide gauge data undertaken by Haigh et al. (2016). A detailed quantitative comparison is not possible given the different methods and datasets used between the two studies. Based on limited tide gauge data, Haigh et al. (2016) identified four categories of skew surge footprints. Their Category 1 events cover the southwest coast and can be comparable with our footprint types 2 and 5. Their Category 2 events cover the west coast of Britain and correspond to our Types 4 and 6. Their Category 3 events cover the coast of Scotland and match our Type 7. Their Category 4 events cover the UK east and southeast coasts and correspond to our Types 1, 3 and 8. Types 2, 4, 5, 6 and 7 represent surge events that also affect the coastlines of Ireland, which were not included in Haigh et al. (2016), allowing a better definition of the spatial extent of the patterns of surge footprints. On the other hand, this approach allows to distinguish patterns of surge footprints that concentrate the impact on different areas of the same coast, as is the case for types T1, T3 and T8 along the east coast of the UK.
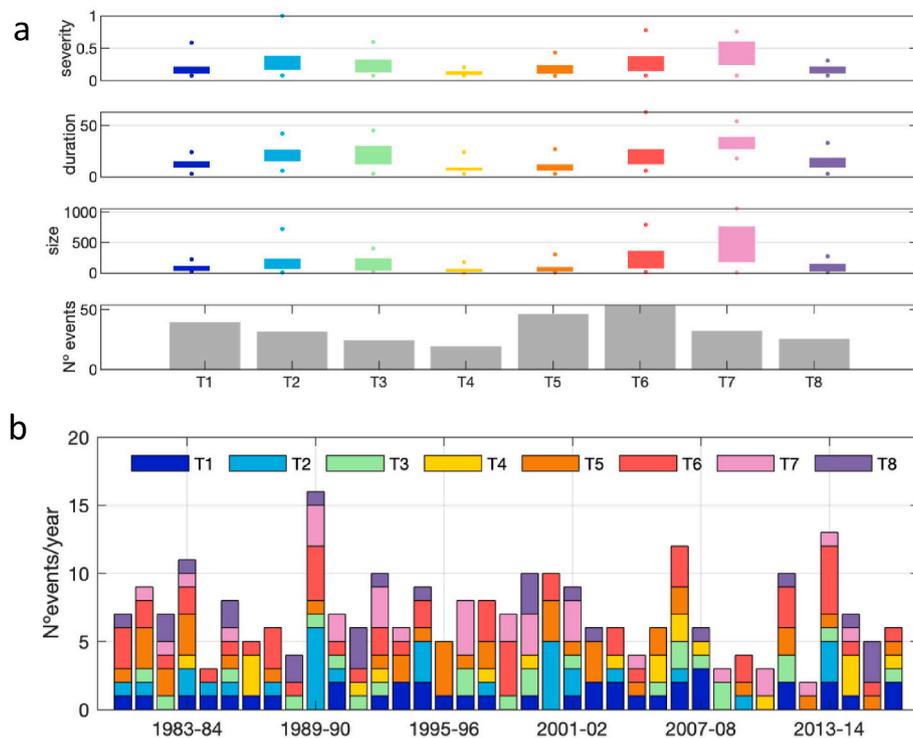
Fig. 9. Characterization of the 8 surge footprint types: (a) severity index, duration (in hours) and footprint size (number of coastal sites with a surge value over TH2 threshold) of the surge events represented by each cluster (the mean, the range between the 25th and 75th percentile, and the maximum and minimum are shown) and the number of events represented by each cluster; c) interannual variability of the 8 types.

We have expanded the study domain compared with Haigh et al. (2016) and some spatial footprints were detected that extend to Ireland, in agreement with the global results of Enríquez et al. (2020). However, our study still has spatial limitations. For example, elevated storm surge levels are known to have occurred on the 5th and December 6, 2013 in other countries in northern Europe (e.g., Netherlands and Germany) (Wadey et al., 2015). In the future, we could expand our study domain further to account for this. Additionally, some surge events affected unconnected areas as Haigh et al. (2016) observed on February 26, 1990, and we detected it, as shown in Fig. 5f. However, our classification of the spatial extreme events has certain limitations to represent specific surge footprints, such as the one occurring on February 26, 1990, which is associated with T7. The KMA is applied to the maximum storm surge during each event at each location, and although it is able to capture the spatial distribution of the surge values, how they are reflected in the return period values is more complex. Each surge footprint type is represented by the mean of the return periods of the corresponding individual spatial surge events and may not be fully representative of all events within that cluster. Ideally, a detailed analysis of each surge event independently is required to capture the complex behaviour of storm surges; nonetheless, a classification still provides useful information.

Regarding the interannual variability, our study highlights the 1989-90 season as the most relevant in terms of the number of extreme spatial surge events and their severities, and it includes the most severe event. However, based on the analysis of the combination of the frequency and intensity of extra-tropical cyclones, Matthews et al. (2014) showed that the 2013-14 season was the stormiest season in the last four decades for the UK. In terms of coastal flooding, Haigh et al. (2016) found that the 2013-14 season contained more extensive events compared to 1989–90. They analysed the characteristics of extreme sea levels, astronomical tides, and skew surges at 40 tide gauges around the coast of the UK. They found that in the tide gauge records, the largest skew surges at 11 of the 40 sites occurred during the 2013-14 season. Four out of these 11 skew surge events in the 2013-14 season ranked in the top 20 events, and seven in the top 35 events, across all 40 sites. We have briefly compared

the dates of some of the largest skew surges registered at the 40 gauges with the dates of the spatial surge events we have identified here, and there is a high level of coherence. During the 5th and December 6, 2013, the largest skew surges in the available tide gauge records were recorded at Whitby (35 in Supplementary Figure SM1), Immingham (36), Lowestoft (38), and Dover (41). Surge levels are also highest along this stretch of coastline in our spatial surge event (see Fig. 3), which is ranked as the 17th most severe event out of the 270. On the December 27, 2013, the largest skew surges were observed in the tide gauge records on the west coast of the Irish Sea (Holyhead (16 in Supplementary Figure SM1), Workington (20), Port Erin (21), Portpatrick (23) tide gauges) which corresponds to the elevated levels in the surge event we identified at this time, which is the 16th most severe event. Moreover, the extreme conditions in 2013-14 were reflected in widespread coastal flooding impacts (Haigh et al., 2017), with the highest number of coastal flooding events registered in the last four decades (13 flooding episodes compared with 5 in 1989-90, see Supplementary Figure SM6). Our analysis in this paper used a surge hindcast driven by the ERA5 reanalysis. Reanalyses are known to contain inhomogeneities in time and space due to the quantity and quality of assimilated data (Hersbach et al., 2020), and these effects are noticeable prior to 1991 (Taszarek et al., 2021), after which there was a rapid increase in the number of assimilated observations available from satellites.

Besides the bias and inconsistent climate variability in the atmospheric reanalysis, numerical surge modelling processes can exacerbate differences further. Although extreme surge events are caused primarily by the horizontal gradient of atmospheric pressure and wind stress at the sea surface (Pugh and Woodworth, 2014), which is conditioned by the intensity and track of the weather system, their magnitude is influenced by other factors such as bathymetry and coastal topography (Williams et al., 2016) and interactions with other sea surface dynamics, such as tides and waves. In this sense, hindcasts, like CoDEC, may lack sufficient bathymetric resolution to simulate the level of local detail captured by tide gauges. Validating the CoDEC dataset with observed sea levels from the tide gauge stations in the Global Extreme Sea Level Analysis (GESLA)
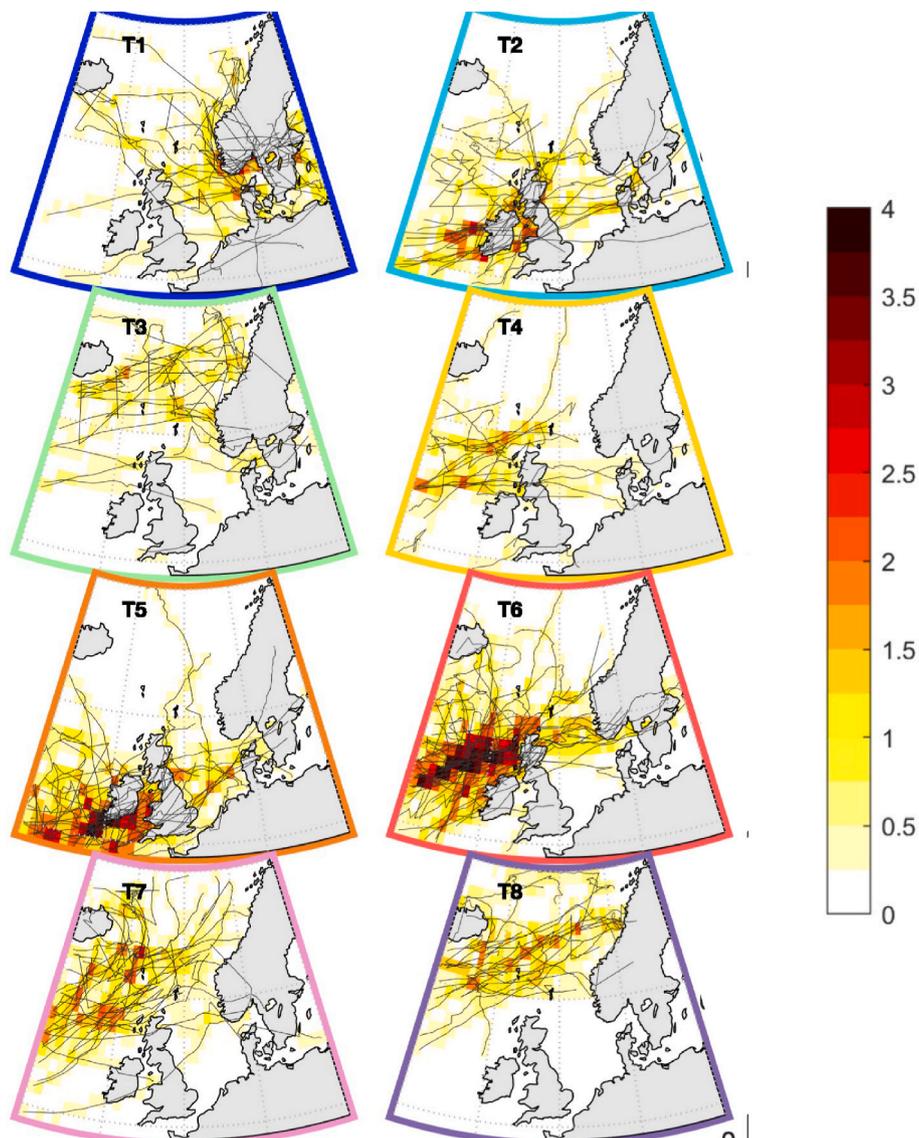
Fig. 10. Storm tracks associated with each footprint type and the corresponding track density (%) calculated as the number of storms that cross each unit area of 1.0° × 1.0° divided by the total number of surge events (M = 270). See Fig. 9 for classification colour schemes.

dataset (Woodworth et al., 2016) demonstrated that CoDEC tends to overestimate the extreme sea levels (>6.0 m) and underestimate sea levels in regions with a high tidal range, such as the North Sea (Muis et al., 2020). Our validation of CoDEC, using 41 tide gauges, also reveals that storm surges are overestimated along the entire coastline of our study domain, except in the Bristol Channel. Although there are no differences between the west and east coasts, the spatial storm surges that impact the west coast tend to be larger and more frequent during the 1989-90 season, which could explain why this season is the dominant in our study. In this context, Jenkins et al. (2023) also observed that the 1989-90 season prevails in the record of extreme surge events in the CoDEC hindcast data, whilst tide gauge measurements suggest that 2013–2014 emerges as the dominant season.

In Haigh et al. (2016), storm tracks were digitalized using an interactive Matlab interface, selecting the grid point of lowest atmospheric pressure at each 6-h time step. We have detected the atmospheric storm tracks that drive the surge events based on a much more sophisticated vortex identification algorithm, but similarities are evident between the two studies. Haigh et al.'s Category 1 matches with our Types 2 and 5 which are generated by storm tracks that pass over mid latitudes of the UK. Category 2, which corresponds with our Types 4 and 6, is associated

with storm tracks that cross through Scotland. Surge events of Type 7, which correspond to Category 3 in Haigh et al. (2016), are generated by storm tracks that pass through higher northern latitudes. In the case of Category 4 in Haigh et al. (2016), which are represented by our Types 12 and 13, in terms of spatial surge events, we can distinguish storm tracks with a west-east direction over the eastern part of the study domain and with north-south direction across the North Sea that were not detected in Haigh et al. (2016).

The proposed tracking algorithm can capture the dependence of the storm surge along the UK/Ireland coastlines, clustering the time series into unique extreme events. These spatial surge events, identified, can be used as inputs to define tail dependence in multivariate extreme value distributions (see, for instance, Diederen et al., 2019). A large catalogue of spatially coherent synthetic event descriptors can be generated from the fitted model. These synthetic extreme surge events can be used as boundary conditions to force coastal hydraulic models to create flood event footprints, which, when intersected with exposure and vulnerability information, can provide estimates of flood risk across asset portfolios (Quinn et al., 2019).

Finally, in this study, for simplicity, we have focused only on the meteorological driven component (i.e., storm surge) of sea level.
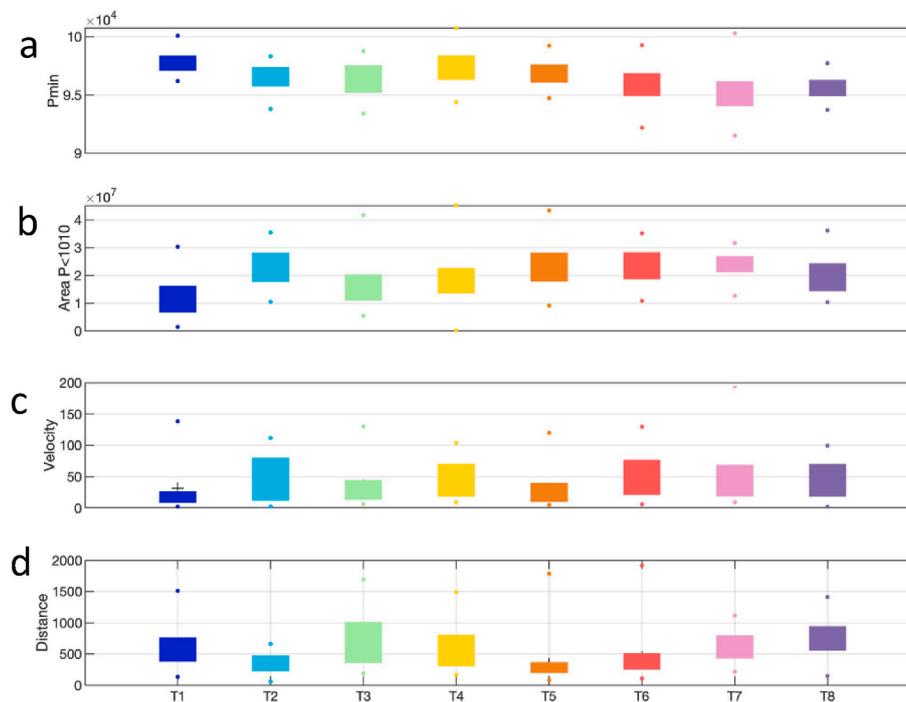
Fig. 11. Characteristics of the storm tracks: a) Pmin, in mbar; b) Area with P < 1010 mbar, in km^2; c) Forward Speed, in km/h; d) Distance, in km, associated with each cluster of surge events. See Fig. 8 for classification colour schemes.

However, coastal flooding arises from extreme sea levels, driven by combinations of storm surges with high astronomical tides. In the future, we hope to extend the analysis and look at the spatial footprints of extreme sea levels, incorporating the astronomical tidal component. Extreme surges may or may not coincide with high astronomical tides but when they do, findings relating to spatial dependence of surges can be used to infer similar spatial characteristics in terms of total sea level and hence coastal flooding.

6. Conclusions

In this paper, we have developed and applied a novel tracking algorithm to a high-resolution storm surge hindcast to identify the spatial footprint of 270 extreme storm surge events around the coast of the UK and Ireland between 1980 and 2017. This approach allow us to characterize each spatial surge event by means of its severity, duration and footprint size. We also examine the tracks and characteristics of the storms responsible for these events. To our knowledge, this is the most detailed spatial and temporal analysis that has been undertaken on storm surges to date. This approach could now easily be undertaken for any coastal region, or even be applied globally.

Our results show that coastlines around the north of the Irish Sea experience the longest and largest surge events while the southwest coast of England is affected by surge events with the shortest durations and smallest footprint sizes. In terms of interannual temporal variability, the winter seasons of 1989-90 and 2013-14 have stood out as the most relevant in terms of the number of events and their severity. The most extreme surge event and the highest number of spatial events occurred in the winter season 1989–90, whilst the proportion of events with larger severity occurred during the winter season 2013–14. We have identified 8 spatial cluster types across the study domain. We have linked these types of spatial surge events with the storm tracks and characteristics that inform which coastal areas could be more likely affected by extreme surges and their severity based on meteorological parameters.

The framework we have developed, and the resulting spatio-temporal characterization of storm surges, will be useful as an input to improve the assessment of coastal flooding risk and can help inform reinsurance, infrastructure reliability and emergency response. For instance, the clustering of historical time series information into unique extreme events can be used to provide training data for stochastic models that generate a large catalogue of extreme surge events for probabilistic flood risk assessment.

CRediT authorship contribution statement

Paula Camus: Writing – review & editing, Writing – original draft, Visualization, Validation, Software, Methodology, Investigation, Formal analysis, Data curation, Conceptualization. **Ivan D. Haigh:** Writing – review & editing, Supervision, Project administration, Funding acquisition, Formal analysis, Conceptualization. **Niall Quinn:** Writing – review & editing, Software, Methodology, Investigation, Formal analysis, Conceptualization. **Thomas Wahl:** Writing – review & editing, Funding acquisition, Formal analysis, Conceptualization. **Thomas Benson:** Writing – review & editing, Software, Funding acquisition, Formal analysis. **Ben Gouldby:** Writing – review & editing, Software, Formal analysis. **Ahmed A. Nasr:** Writing – review & editing, Methodology, Formal analysis. **Md Mamunur Rashid:** Writing – review & editing, Methodology, Formal analysis. **Alejandra R. Enríquez:** Writing – review & editing, Methodology, Formal analysis. **Stephen E. Darby:** Writing – review & editing, Formal analysis. **Robert J. Nicholls:** Writing – review & editing, Formal analysis. **Norberto C. Nadal-Caraballo:** Writing – review & editing, Formal analysis.

Declaration of competing interest

The authors declare that they have no known competing financial interests or personal relationships that could have appeared to influence the work reported in this paper.

Data availability

Data will be made available on request.

Acknowledgements

Appendix A. Supplementary data

Supplementary data to this article can be found online at https://doi.org/10.1016/j.wace.2024.100662.

References

Anderson, D., Rueda, A., Cagigal, L., Antolinez, J.A.A., Mendez, F.J., Ruggiero, P., 2019. Time-varying emulator for short and long-term analysis of coastal flood hazard potential. J. Geophys. Res.: Oceans 124, 9209–9234. https://doi.org/10.1029/2019JC015312.

Arns, A., Wahl, T., Wolff, C., et al., 1918. Non-linear interaction modulates global extreme sea levels, coastal flood exposure, and impacts. Nat. Commun. 11, 2020. https://doi.org/10.1038/s41467-020-15752-5.

Bertin, X., Li, K., Roland, A., Bidlot, J., 2015. The contribution of shortwaves in storm surges: two case studies in the bay of Biscay. Continental. Shelf. Res. 96, 1–15. https://doi.org/10.1016/j.csr.2015.01.005.

Camus, P., Haigh, I.D., Nasr, A.A., Wahl, T., Darby, S.E., Nicholls, R.J., 2021. Regional analysis of multivariate compound coastal flooding potential around Europe and environs: sensitivity analysis and spatial patterns. Nat. Hazards Earth Syst. Sci. 21, 2021–2040. https://doi.org/10.5194/nhess-21-2021-2021.

Camus, P., Menéndez, M., Méndez, F.J., Izaguirre, C., Espejo, A., Cánovas, V., Pérez, J., Rueda, A., Losada, I.J., Medina, R., 2014. A weather-type statistical downscaling framework for ocean wave climate. J. Geophys. Res. https://doi.org/10.1002/2014JC010141.

Diederen, D., Liu, Y., Gouldby, B., Diermanse, F., Vorogushyn, S., 2019. Stochastic generation of spatially coherent river discharge peaks for continental event-based flood risk assessment. Nat. Hazards Earth Syst. Sci. 19 (5), 1041–1053. https://doi.org/10.5194/nhess-19-1041-2019.

Dullaart, J.C.M., Muis, S., Bloemendaal, N., et al., 2021. Accounting for tropical cyclones more than doubles the global population exposed to low-probability coastal flooding. Commun Earth Environ 2 (135). https://doi.org/10.1038/s43247-021-00204-9.

Eilander, D., Couasnon, A., Ikeuchi, H., Muis, S., Yamazaki, D., Winsemius, H.C., Ward, P.J., 2020. The effect of surge on riverine flood hazard and impact in deltas globally. Environ. Res. Lett. 15 (10), 104007 https://doi.org/10.1088/1748-9326/ab8ca6.

Endrikat, S.. Find vortices in velocity fields. https://www.mathworks.com/matlabcentral/fileexchange/52343-find-vortices-in-velocity-fields. (Accessed 15 December 2020). MATLAB Central File Exchange.

Enríquez, A.R., Wahl, T., Marcos, M., Haigh, I.D., 2020. Spatial footprints of storm surges along the global coastlines. J. Geophys. Res.: Oceans 125 (9), e2020JC016367. https://doi.org/10.1029/2020jc016367.

Graftieaux, L., Michard, M., Grosjean, N., 2001. Combining PIV, POD and vortex identification algorithms for the study of unsteady turbulent swirling flows. Meas. Sci. Technol. 12 (9), 1422–1429. https://iopscience.iop.org/article/10.1088/0957-0233/12/9/307/pdf.

Haigh, I.D., Ozsoy, O., Wadey, M.P., Nicholls, R.J., Gallop, S.L., Wahl, T., Brown, J.M., 2017. An Improved Database of Coastal Flooding in the United Kingdom from 1915 to 2016, vol. 4. press Scientific Data, 170100.

Haigh, I.D., Wadey, M.P., Wahl, T., Ozsoy, O., Nicholls, R.J., Brown, J.M., et al., 2016. Spatial and temporal analysis of extreme sea level and storm surge events around the coastline of the UK. Sci. Data 3 (November), 1–23. https://doi.org/10.1038/sdata.2016.107.

Hersbach, H., Bell, B., Berrisford, P., Hirahara, S., Horányi, A., Muñoz-Sabater, J., Nicolas, J., Peubey, C., Radu, R., Schepers, D., Simmons, A., Soci, C., Abdalla, S., Abellan, X., Balsamo, G., Bechtold, P., Biavati, G., Bidlot, J., Bonavita, M., De Chiara, G., Dahlgren, P., Dee, D., Diamantakis, M., Dragani, R., Flemming, J., Forbes, R., Fuentes, M., Geer, A., Haimberger, L., Healy, S., Hogan, R.J., Hólm, E., Janisková, M., Keeley, S., Laloyaux, P., Lopez, P., Lupu, C., Radnoti, G., de Rosnay, P., Rozum, I., Vamborg, F., Villaume, S., Thépaut, J.-N., 2020. The ERA5 global reanalysis. Q. J. R. Meteorol. Soc. 146 (730), 1999–2049.

Horsburgh, K.J., Wilson, C., 2007. Tide-surge interaction and its role in the distribution of surge residuals in the North Sea. J. Geophys. Res. 112, C08003.

HR Wallingford/USACE, 2022. Extratropical Storm Tracks: East Coast of the USA. HR Wallingford report FWR6396-RT001-R02-00, undertaken on behalf of the US Army Corps of Engineers, February.

Idier, D., Bertin, X., Thompson, P., et al., 2019. Interactions between mean Sea Level, tide, surge, waves and flooding: mechanisms and contributions to Sea Level variations at the coast. Surv. Geophys. 40, 1603–1630. https://doi.org/10.1007/s10712-019-09549-5.

Idier, D., Dumas, F., Muller, H., 2012. Tide-surge interaction in the English channel. Nat. Hazards Earth Syst. Sci. 12, 3709–3718.

Jenkins, L.J., Haigh, I.D., Camus, P., et al., 2023. The temporal clustering of storm surge, wave height, and high sea level exceedances around the UK coastline. Nat. Hazards 115, 1761–1797. https://doi.org/10.1007/s11069-022-05617-z.

Kernkamp, H.W.J., Van Dam, A., Stelling, G.S., de Goede, E.D., 2011. Efficient scheme for the shallow water equations onunstructured grids with application to the Continental Shelf. Ocean Dynam. 61, 1175–1188.

Kirezci, E., et al., 2020. Projections of global-scale extreme sea levels and resulting episodic coastal flooding over the 21st century. Sci. Rep. 10, 1–12.

Lavaud, L., Bertin, X., Martins, K., Arnaud, G., Bouin, M.-N., 2020. The contribution of short-wave breaking to storm surges: the case klaus in the southern bay of biscay. Ocean Model. 156, 101710 https://doi.org/10.1016/j.ocemod.2020.101710.

Matthews, T., Murpy, C., Wilby, R.L., Harrigan, S., 2014. Stormiest winter on record for Ireland and UK. Nat. Clim. Change 4, 738–740. https://doi.org/10.1038/nclimate2336.

Mastenbroek, C., Burgers, G., Janssen, P.A.E.M., 1993. The dynamical coupling of a wave model and a storm surge model through the atmospheric boundary layer. J. Phys. Oceanogr. 23, 1856–1867.

Muis, S., et al., 2020. A high-resolution global dataset of Extreme Sea levels, tides, and storm surges, including future projections. Front. Mar. Sci. 7, 263. https://doi.org/10.3389/fmars.2020.00263.

Pedreros, R., Idier, D., Muller, H., Lecacheux, S., Paris, F., Yates, M., et al., 2018. Relative contribution of wave setup to the storm surge: observations and modelling based analysis in open and protected environments (truc vert beach and tubuai island). J. Coast Res. 85 (1), 1046–1050. https://doi.org/10.2112/SI85-210.

Pineau-Guillou, L., Bouin, M.N., Ardhuin, F., Lyard, F., Bidlot, J., Chapron, B. Impact of wave-dependent stress on storm surge simulations in the North Sea: ocean model evaluation against in situ and satellite observations. Ocean Model., 154, pp.101694-, 10.1016, 2020,/j.ocemod.2020.101694. hal-03492307.

Pugh, D., Woodworth, P., 2014. Sea-Level Science: Understanding Tides, Surges, Tsunamis and Mean Sea-Level Changes. Cambridge Univ. Press, Cambridge, U. K.

Quinn, N., Bates, P.D., Neal, J., Smith, A., Wing, O., Sampson, C., et al., 2019. The spatial dependence of flood hazard and risk in the United States. Water Resour. Res. 55, 1890–1911. https://doi.org/10.1029/2018WR024205.

Spencer, T., Brooks, S.M., Evans, B.R., Tempest, J.S., Möller, I., 2015. Southern North Sea storm surge event of 5 December 2013: water levels, waves and coastal impacts. Earth Sci. Rev. 146, 120–145. https://doi.org/10.1016/j.earscirev.2015.04.002.

Stephens, S.A., Bell, R.G., Haigh, I., 2020. Spatial and temporal analysis of extreme stormtide and skew-surge events around the coastline of New Zealand. Natural Hazards Earth Syst. Sci. Discuss 20 (3), 783–796.

Taszarek, M., Pilguj, N., Allen, J.T., Gensini, V., Brooks, H.E., Szuster, P., 2021. Comparison of convective parameters derived from ERA5 and MERRA-2 with rawinsonde data over Europe and north America. J. Clim. 34 (8), 3211–3237.

Thomas, A., Dietrich, J.C., Asher, T.G., Bell, M., Blanton, B.O., Copeland, J.H., Cox, A.T., Dawson, C.N., Fleming, J.G., Luettich, R.A., 2019. Influence of storm timing and forward speed on tides and storm surge during Hurricane Matthew. Ocean Model. 137, 1–19. https://doi.org/10.1016/j.ocemod.2019.03.004. ISSN 1463-5003.

Ullrich, P.A., Zarzycki, C.M., 2017. TempestExtremes: a framework for scale-insensitive pointwise feature tracking on unstructured grids. Geosci. Model Dev. (GMD) 10, 1069–1090. https://doi.org/10.5194/gmd-10-1069-2017.

Vousdoukas, M.I., et al., 2018. Global probabilistic projections of extreme sea levels show intensification of coastal flood hazard. Nat. Commun. 9, 2360.

Wadey, M., et al., 2015. A comparison of the 31 January–1 February 1953 and 5–6 December 2013 coastal flood events around the UK. Front. Mar. Sci. 2 (84).

Wing, O.E.J., Quinn, N., Bates, P.D., Neal, J.C., Smith, A.M., Sampson, C.C., et al., 2020. Toward global stochastic river flood modeling. Water Resour. Res. 56, e2020WR027692 https://doi.org/10.1029/2020WR027692.

Woodworth, P.L., Hunter, J.R., Marcos, M., Caldwell, P., Menéndez, M., Haigh, I., 2016. Towards a global higher-frequency sea level dataset. Geoscience Data J 3, 50–59. https://doi.org/10.1002/gdj3.42.

Zscheischler, J., Martius, O., Westra, S., et al., 2020. A typology of compound weather and climate events. Nat. Rev. Earth Environ. 1, 333–347. https://doi.org/10.1038/s43017-020-0060-z.

Zigunov, F.. 2D vortex Core tracking - gamma 1 - super fast. https://www.mathworks.com/matlabcentral/fileexchange/72092-2d-vortex-core-tracking-gamma-1-super-fast. (Accessed 15 December 2020). MATLAB Central File Exchange.